International Journal of Heat and Mass Transfer 52 (2009) 5423–5432

Contents lists available at ScienceDirect

International Journal of Heat and Mass Transfer

journal homepage: www.elsevier.com/locate/ijhmt

Nonlinear analysis on dynamic behavior of buoyancy-induced flame oscillation under swirling flow

Hiroshi Gotoda [a,*], Yuta Asano [a], Keng Hoo Chuah [b], Genichiro Kushida [c]

[a] Department of Mechanical Engineering, Ritsumeikan University, 1-1-1 Nojihigashi, Kusatsu-shi, Shiga 525-8577, Japan
[b] Department of Mechanical Engineering, University of Kentucky, Lexington, KY 40506, USA
[c] Department of Mechanical Engineering, Aichi Institute of Technology, 1247 Yachigusa, Yagusa-cho, Toyota, Aichi 470-0392, Japan

ARTICLE INFO

Article history:
Received 4 March 2009
Received in revised form 5 June 2009
Accepted 26 June 2009
Available online 14 August 2009

Keywords:
Diffusion flame
Buoyancy
Chaos
Swirling flow

ABSTRACT

From the viewpoint of nonlinear dynamics, the dynamic behavior of buoyancy-induced flame oscillation has been experimentally investigated under a swirling flow produced by rotating a cylindrical burner tube. As the rotational Reynolds number increases, the dynamic behavior undergoes a significant transition from periodic oscillation to low-dimensional deterministic chaos, through quasi-periodic oscillation. This is clearly demonstrated by nonlinear time series analysis based on chaos theory. The motion of the vortical structure around the burner tube due to the centrifugal instability associated with a rotating Taylor–Couette flow plays an important role in the onset of low-dimensional deterministic chaos.

© 2009 Elsevier Ltd. All rights reserved.

1. Introduction

Combustion phenomena are among the most typical thermal flows associated with a rapid chemical reaction, and have inherently strong nonlinearity of the turbulent flow and chemical kinetics (e.g., the exponential dependence of reaction rate on temperature). Therefore, the periodic and chaotic motion in flame dynamics that can be observed as a result of flame instabilities are of fundamental importance to present-day combustion physics and thermal fluid science research. The buoyant force driven by natural convection under terrestrial gravity is one of the most significant factors for generating and growing flame instabilities. In diffusion flames, the entire flow field predominantly consists of hot combustion products (light gas) behind the flame front and cold surrounding air (heavy gas). When hot combustion products accelerated by an upward buoyant force interact with the cold surrounding air, the interface between these fluids becomes unstable owing to the hydrodynamic shear layer instability associated with the Kelvin–Helmholtz instability mechanism, resulting in a large-scale toroidal vortex at the interface [1,2]. As the large-scale toroidal vortex develops and moves downstream, it interacts with the flame front to distort the flame shape and induce large oscillations in amplitude owing to the Rayleigh–Taylor instability mechanism [3]. The periodic oscillation of the flame front generated by these processes is referred to as the *flickering flame*, and its dynamics is significant for understanding the transition from a laminar to turbulent flame. Thus far, many aspects of flame oscillations/buoyancy interaction for the flickering flame originating from circular nozzles have been extensively investigated at different gravitational strengths [4,5], pressures [6], and oxygen concentrations of the surrounding gas [7,8]. However, the dynamic behavior of buoyancy-induced flame oscillation has not been fully investigated under a swirling flow, which is one of the most significant flow configurations in fundamental combustion systems. This subject includes fascinating flame instability issues generated by buoyancy/swirl coupling that have not been discussed in past studies [1–8]. In fact, regarding the buoyancy-induced flame oscillation of a swirling jet diffusion flame at a low Reynolds number, Huang and Yen [9] recently showed that an annular air jet with a low swirl is insensitive to changes in the structure of a buoyancy-driven large-scale toroidal vortex at the shear layer, but the breakdown of the large-scale toroidal vortex due to a strong swirl produces a chaotic flow field, resulting in the formation of a lifted fluctuating flame as the precursor to a turbulent flame.

A rotating cylindrical burner that spins on its central axis is one of the most fundamental burners for investigating the effects of both buoyancy and centrifugal force on flame dynamics under a laminar flow condition [10–12]. This configuration makes it feasible to independently and systematically control the initial jet momentum of the fuel and the centrifugal force. In our preliminary work [13], in which the rotating cylindrical burner was used, we observed that under a low swirling flow, the buoyancy-induced periodic oscillation of the flame front remains unchanged, but it

* Corresponding author.
E-mail address: gotoda@se.ritsumei.ac.jp (H. Gotoda).

0017-9310/$ - see front matter © 2009 Elsevier Ltd. All rights reserved.
doi:10.1016/j.ijheatmasstransfer.2009.06.035

Nomenclature

$C(:)$	correlation integral
d_i	diameter of burner tube (mm)
d_o	diameter of Pyrex glass chimney (mm)
D	embedding dimension
D_c	correlation dimension
f_b	oscillation frequency generated by buoyancy-driven hydrodynamic instability (Hz)
f_c	collision frequency of Taylor-like vortices (Hz)
$H(:)$	information entropy (bit)
$H(:,:)$	joint information entropy (bit)
I	mutual information (bit)
n	data number of time series of deviation from mean flame front location
n_c	number of collisions
N	rotational speed of burner tube (rpm)
$p(:)$	probability density function
$p(:,:)$	joint probability density function
r	radial coordinate
r_f	flame front location in radial direction at location (mm)
$\bar{r}_f$	time-averaged flame front location (mm)
Re_j	Reynolds number of fuel jet
Re_r	rotational Reynolds number of burner tube
S	Swirl number
t_i	time at ith data point of time series of Δr_f (s)
t_j	time at which Taylor-like vortex collides with flame base (s)
T	time of laser tomographic images (s)
u	random variable
u_j	axial velocity of fuel jet (m/s)
v	random variable
v_θ	tangential velocity at surface of burner tube (m/s)
U	set of realizations of random variable
V	set of realizations of random variable
V_f	bulk fuel injection velocity (m/s)
$\boldsymbol{X_i}$	constructed phase space vectors at time t_i
$\boldsymbol{X_j}$	constructed phase space vectors with exception of $\boldsymbol{X_i}$
z	vertical coordinate

Greek symbols

ν_f	kinematic viscosity coefficient of fuel (m^2/s)
ν_a	viscosity coefficient of surrounding air (m^2/s)
ρ_f	density of fuel (kg/m^3)
ω	angular velocity of burner tube (rad/s)
τ	time delay (s)
τ_0	suitable time lag for constructing D-dimensional phase space (s)
ε	radius of D-dimensional hypersphere in phase space
$\Theta(:)$	Heaviside function
Δr_f	deviation from mean flame front location (mm)
$\Delta r_f(t_i)$	deviation from mean flame front location at time t_i (mm)

switches to nonperiodic oscillation that is thought to be chaotic but not turbulent under a high swirling flow. Our recent numerical investigation [14] showed that the vortex motion generated by the centrifugal instability associated with a rotating Taylor–Couette flow may cause irregular fluctuations in the flame front dynamics. Therefore, it is interesting to reveal how the transition from periodic to nonperiodic oscillation in the flame front dynamics changes with the swirling flow. A nonlinear time series approach inspired by chaos theory is becoming an increasingly reliable tool for clarifying the nonlinear characteristics of complex dynamics in a dissipative system. In thermal science, nonlinear time series analysis has been widely applied to study unstable fluid motion in a heated air flow [15], two-phase flows through a T-junction [16], unstable boiling in a microchannel [17], and bubbling behavior [18–20] in recent years. Regarding flame instability, we have demonstrated the suitability of nonlinear time series analysis for characterizing and predicting the dynamic behavior of an unstable fluctuating premixed flame [21–23]. The investigation of the dynamic behavior of the flame instability observed in this study by a sophisticated nonlinear time series analysis is extremely important for gaining a more comprehensive understanding and interpretation of the complex nonlinear phenomena in flame dynamics. Nevertheless, this interesting issue has not been extensively explored in the fields of combustion science and physics.

The main purpose of this study is to conduct a more comprehensive investigation of the dynamic behavior of buoyancy-induced flame oscillation under a swirling flow produced by a rotating cylindrical burner tube, using nonlinear time series analysis for time series data of the fluctuations of the flame front. This paper is organized as follows. In Section 2, the experimental system and method used in this work are described. In Section 3, we present the central ideas behind the mathematics of nonlinear time series analysis. Experimental results are presented and discussed in Section 4. We present our conclusions in Section 5.

2. Experimental apparatus and method

The rotating cylindrical burner used in this work is shown schematically in Fig. 1. The fuel flows through a diffuser, a honeycomb, fine damping screens, a nozzle, and a burner tube (with diameter d_i = 10 mm). The burner tube is supported vertically by bearings and is rotated by a DC motor through a pulley and belt unit. When the burner tube is rotated, both the surface of the burner tube and the fuel jet are rotated simultaneously. A 25 mm height honeycomb section with a grid diameter of 1.04 mm is fitted inside the burner tube to induce the solid-body rotation of the fuel at the burner tube exit. In addition to the above burner tube, we use a burner tube that the surface of the burner tube does not rotate (Note that the solid-body rotation is induced in the fuel flow without rotating the surface of the burner tube.) in order to investigate the effect of the vortex motion generated by the centrifugal instability on the flame dynamics, as mentioned in Section 4. Methane (CH_4) was used as the fuel in this work. The bulk fuel injection velocity (=volume flow rate/cross-sectional area of the burner tube) V_f was varied from 0.10 to 0.25 m/s in the current experiment because it was under these conditions that the axisymmetric buoyancy-driven flickering flame was formed for the non-swirling case. The Reynolds number Re_j ($=V_f d_i/\nu_f$, where ν_f is the kinematic viscosity coefficient of the fuel) was between 58 and 144. The rotational speed of the burner tube N was varied from 0 to 1400 rpm (23.3 s^{-1}) at 200 rpm intervals. The rotational Reynolds number Re_r was between 0 and 549 ($Re_r = v_\theta d_i/\nu_a$, where v_θ is the tangential velocity at the surface of the burner tube exit (r = 5 mm) and ν_a is the viscosity coefficient of the surrounding air). To characterize the balance between the axial momentum and the swirl momentum of the fuel, the Swirl number S was introduced ($S = 2\pi \int_0^{d_i/2} \rho_f u_j v_\theta r^2 dr / 2\pi R \int_0^{d_i/2} \rho_f u_j^2 r dr = \omega d_i / V_f$, where u_j is the axial velocity of the fuel, ρ_f is the density of the fuel and ω ($=\pi N/30$) is the angular velocity of the burner tube).

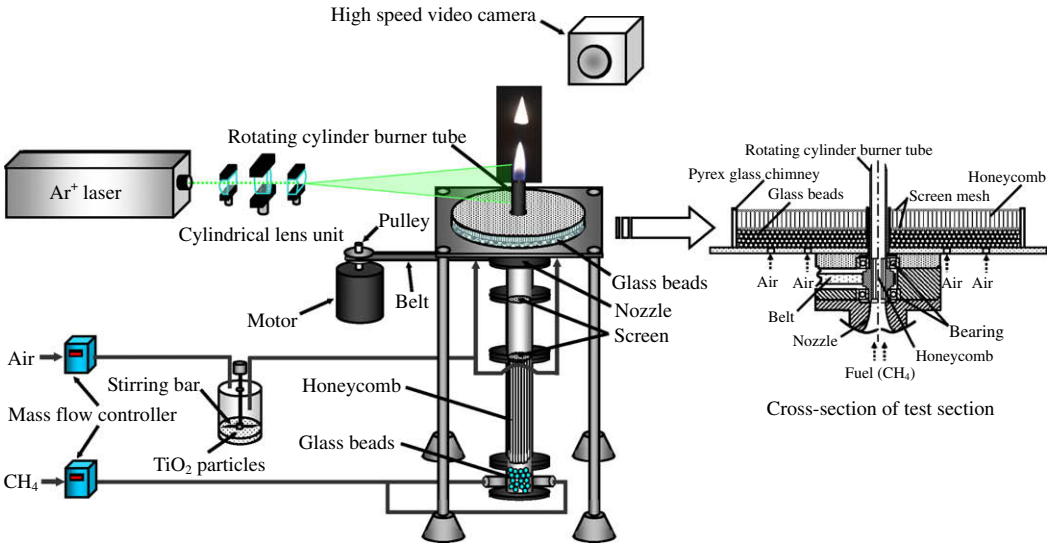

Fig. 1. Schematic of experimental system.

To investigate the dynamic behavior of the flame front, the time variation of the flame front location r_f (mm) in the radial direction at a location (z = 20 mm) close to the flame base was measured as shown in Fig. 2. Note that the time variation of r_f at z = 20 mm is synchronized with that of r_f at the higher location of z = 30 mm. The former measurement location has physical significance for discussing the dynamic behavior of the flame front, because flame oscillation is initiated around the flame base by the hydrodynamic shear layer instability of the interface between the hot combustion products and the cold surrounding air. In addition, as mentioned in Section 4, the vortex motion generated by the centrifugal instability affects the flame base, resulting in the chaotic oscillation of the flame front. Therefore, the flame front location of z = 20 mm was used for measurement as an important location for investigating the dynamic behavior of the flame front. The flame front around the flame base was recorded at 1000 frames per second by a high-speed video camera (Photron 1024 PCI) with a frame size of 1024 × 1024 pixels. The spatial resolution of the images was 25 pixels per millimeter, which was sufficient for analyzing the flame front dynamics. The deviation from the mean flame front location $\Delta r_f = r_f - \bar{r}_f$ was measured as a function of time t. Here, $\bar{r}_f$ is the time-averaged flame front location. The sampling frequency of the obtained time series was 1 kHz, and the data number n was 10,000. Nonlinear time series analysis was applied to the time variation of Δr_f, as discussed in Section 3.

A laser tomographic method was used in this study to visualize the change in the flow field around the flame base generated by the centrifugal instability. The light source was an Ar^+ laser (LEXEL Model 95) with a maximum power of 2 W. An optical unit shaped the laser beam into a sheet with a thickness of approximately 0.5 mm, and the laser sheet then traversed the test section. The Mie scattered light emitted from TiO_2 particles that were seeded in the airflow were visualized. The air was issued with a low speed of 0.005 m/s from the bottom of a Pyrex glass chimney (d_o = 200 mm) positioned outside the rotating burner tube and did not affect the flow field around the burner tube. A damping screen, glass beads, and a honeycomb were set in the chimney to ensure the uniformity of the airflow inside the outer chimney. The visualized images were recorded with a high-speed video camera at 1000 frames per second.

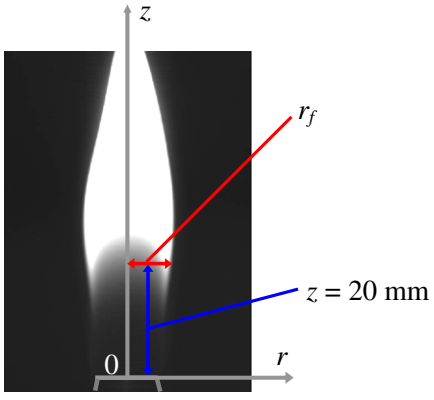

Fig. 2. Definition of flame front location.

3. Mathematical treatment used for time series analysis

As mentioned in Section 1, nonlinear time series analysis is important for gaining a comprehensive understanding of complex nonlinear phenomena and has been widely applied to study the dynamic behavior of thermofluid phenomena. However, it has not been applied to the investigation of combustion phenomena. The central idea behind the mathematics of the method of time series analysis employed in this work is briefly described in the following subsections.

3.1. Mutual information

Mutual information, defined below and introduced by Fraser and Swinney [24], is a function of the time distance between the data points of a time series and provides useful information for determining the optimal time lag for embedding as well as measuring the rate of spontaneous decay of information from the time series. Let U and V be sets of realizations of the random variables u and v, respectively. We approximate the probability density functions $p(u)$ and $p(v)$ one-dimensional histograms and the joint probability density function $p(u, v)$ with a two-dimensional histogram generated from sets of sample data $\{u_i\}_{i=1}^n$ and $\{v_i\}_{i=1}^n$. The infor-

mation entropies $H(U)$ and $H(V)$ and the joint information entropy $H(U, V)$ are calculated using

$$H(U) = -\sum_{i=1}^{n} p(u_i)\log_2 p(u_i) \tag{1}$$

$$H(V) = -\sum_{i=1}^{n} p(v_i)\log_2 p(v_i) \tag{2}$$

$$H(U,V) = -\sum_{ij=1}^{n} p(u_i, v_j)\log_2 p(u_i, v_j) \tag{3}$$

The average mutual information $I(V; U)$ is given by

$$I(V;U) = H(U) + H(V) - H(U,V) \tag{4}$$

where $I(V; U)$ represents the amount of information that one can know about V given U. In this work, the time series $\{\Delta r_f(t_i)\}_{i=1}^{n-\tau}$ is substituted into U and its time-delayed counterpart $\{\Delta r_f(t_i+\tau)\}_{i=1}^{n-\tau}$ is substituted into V. Thus, the mutual information I is a function of the time lag τ and represents the spontaneous loss of information caused by the time evolution of the system in terms of τ. The exponential decay of I can indicate chaos.

3.2. Attractor and correlation dimension

On the basis of Takens' embedding theorem [25], the attractor is constructed from the time series of the deviation from the mean flame front location Δr_f. The time-delayed coordinates used for the construction of the attractor are expressed as

$$X_i = (\Delta r_f(t_i), \Delta r_f(t_i + \tau_0), \ldots, \Delta r_f(t_i + (D-1)\tau_0)) \tag{5}$$

where $i = 0, 1, \ldots, n$ (n is the data number of the time series), $\boldsymbol{X_i}$ are the constructed phase space vectors, $\Delta r_f(t_i)$ is the deviation from the mean flame front location at time t_i, D is the embedding dimension, that is, the dimension of the constructed phase space, and τ_0 is a suitable time lag. If the time lag is too small, then the elements of the phase space vectors are strongly correlated. If the time lag is too large, then the correlation is lost completely. In this work, τ_0 is set to be either the time lag that yields a local minimum of mutual information I or the time lag that reduces I to below e^{-1}, in accordance with the prescription of Fraser and Swinney [24].

A standard and classical method for evaluating the complexities of dynamic behavior is the Grassberger–Procaccia (GP) algorithm [26,27], which enables the estimation of the correlation dimension (a type of fractal dimension) of a geometrical object formed from trajectories in the phase space constructed from time series data. This algorithm has been widely used in previous studies with respect to combustion instabilities [21,23,28]. First, we calculate the two-point correlation function defined as

$$C(\varepsilon) = \frac{1}{N^2}\sum_{\substack{ij=1 \\ i\neq j}}^{N} \Theta(\varepsilon - \|\mathbf{X}_i - \mathbf{X}_j\|) \tag{6}$$

$$\|\mathbf{X}_i - \mathbf{X}_j\| = \sqrt{\sum_{q=1}^{D}(\Delta r_f(t_i + (q-1)\tau_0) - \Delta r_f(t_j + (q-1)\tau_0))^2} \tag{7}$$

where ε is the small radius of the D-dimensional hypersphere in the phase space used for counting the neighboring points. $\|\boldsymbol{X_i} - \boldsymbol{X_j}\|$ represents the Euclidean distance between vectors $\boldsymbol{X_i}$ and $\boldsymbol{X_j}$ in the phase space. $\Theta(x)$ is the Heaviside function ($\Theta(x) = 1$ if $x > 0$; $\Theta(x) = 0$ if $x < 0$).

The value of the Heaviside function is unity if the distance between $\boldsymbol{X_i}$ and $\boldsymbol{X_j}$ is within ε and zero otherwise. A hypersphere of radius ε is centered on one of the $\boldsymbol{X_i}$ vectors. The hypersphere itself is moved from point to point along the trajectories of the phase space. The correlation integral scales with the hypersphere radius ε according to the power law $C(\varepsilon) \approx \varepsilon^{D_c}$, where D_c is the correlation dimension. The correlation dimension can then be estimated from the slope of the linear part of the $\log C(\varepsilon)$ versus $\log \varepsilon$ curve using

$$D_c = \lim_{\varepsilon \to 0} \frac{\log C(\varepsilon)}{\log \varepsilon} \tag{8}$$

4. Results and discussion

The changes in flame motion as functions of the Reynolds number of the fuel jet Re_j and the rotational Reynolds number of the burner tube Re_r are shown in Fig. 3. For the non-swirling flame ($Re_r = 0$), a typical flickering flame with flame-tip separation is clearly formed and generated by the buoyancy-driven hydrodynamic shear layer instability associated with the interface between hot combustion products and the cold surrounding air [1–3]. This periodic oscillation remains nearly unchanged with increasing Re_r up to 156, which indicates that the swirling flow produced by burner rotation is not sufficiently large to alter the buoyancy-driven hydrodynamic instability mechanism. In contrast, when Re_r exceeds 312, an interesting flame with a spirally curved configuration (spiral flame) begins to appear, and the flame motion switches back and forth between the non-axisymmetric flickering flame and the spiral flame. With a further increase in Re_r, the formation of the spiral flame becomes increasingly prominent and the flame front fluctuates irregularly with nonperiodic oscillation that is thought to be chaotic. This transition from the periodic oscillation to the nonperiodic oscillation of the flame front is of great interest in terms of flame instability under a swirling flow, and is the most interesting phenomenon in this work. Another important point to note in Fig. 3 is that the value of N for the onset of the spiral flame is constant even with changes in bulk flow velocity. The reason for appearance of the spiral flame at a specific Re_r (=312) is discussed later on the basis of the result of flow visualization around the burner tube exit.

The deviation from the mean flame front location Δr_f as a function of time t and the power spectrum obtained by fast Fourier transform (FFT) analysis are shown in Fig. 4. Here, the Reynolds

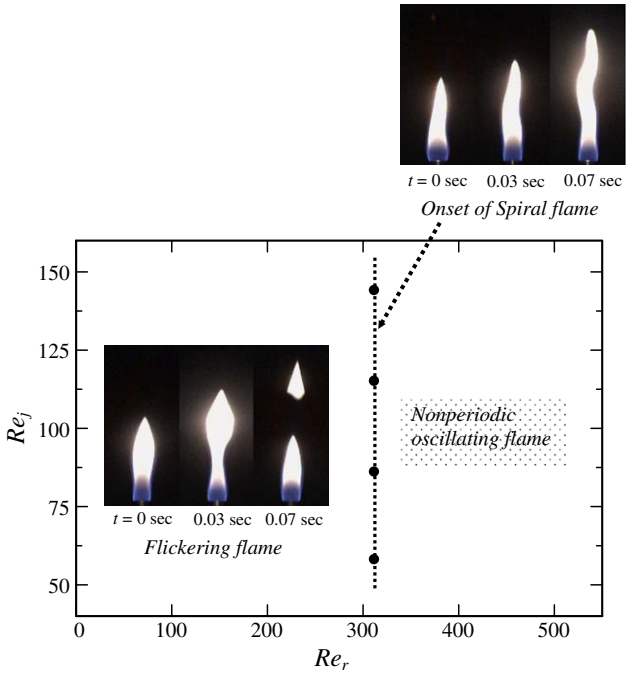

Fig. 3. Changes in flame motion as functions of the Reynolds number of the fuel jet Re_j and the rotational Reynolds number of the burner tube Re_r.

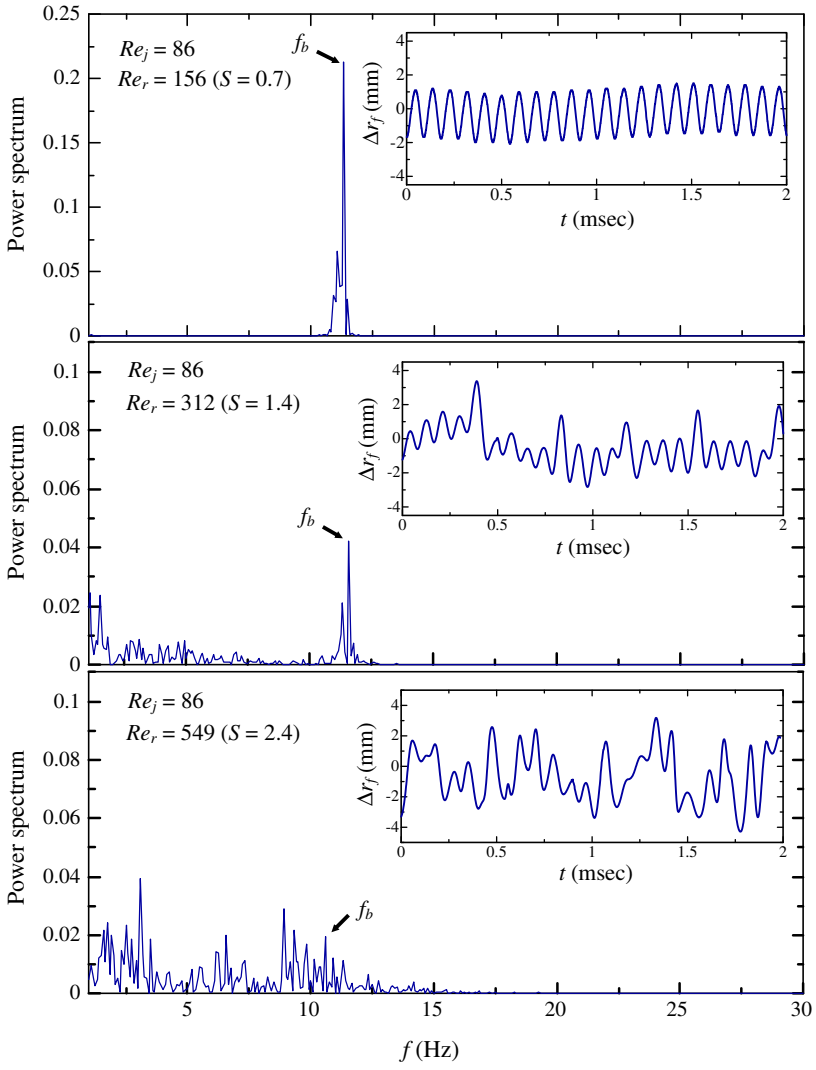

Fig. 4. Time variation of deviation from mean flame front location Δr_f and the power spectrum at Re_j = 86.

number of the fuel jet Re_j = 86 (the fuel injection velocity at the burner tube exit is V_f = 0.15 m/s) is selected for the time series analysis as a representative case in this work. At the rotational Reynolds number of the burner tube Re_r = 156 (Swirl number S = 0.7), periodic oscillation with a distinct peak f_b at 11.2 Hz is clearly observed, corresponding to the time sequence shown in the inset of Fig. 4. f_b is nearly consistent with the oscillation frequency generated by the buoyancy-driven hydrodynamic instability. This trend is similar to that obtained in the non-swirling case (S = 0), and the flame motion does not significantly change with the swirling condition up to S = 0.7. When Re_r reaches 312 (S = 1.4), in addition to the periodic oscillation, many oscillation frequencies with small amplitude appear over a wide range of low-frequency bands owing to the occurrence of the spiral flame. One interesting point is that the value of f_b generated by the buoyancy-driven hydrodynamic instability still persists in the flame front dynamics. This means that the irregular fluctuations induced by the onset of the spiral flame are superimposed on the predominant periodic oscillation, resulting in the complex behavior of the flame dynamics leading to nonperiodic oscillation. With the further increase in Re_r to 549 (S = 2.4), the irregularities of Δr_f become more marked with larger fluctuations. Interestingly, note that the flame oscillation generated by the buoyancy-driven hydrodynamic instability is still discernible in the spectra. These results demonstrate that the buoyancy-driven hydrodynamic instability significantly affects the flame dynamics under a high swirling flow.

The mutual information I as a function of time lag τ at Re_j = 86 is shown in Fig. 5. For Re_r = 156 (S = 0.7), both a large peak and a small

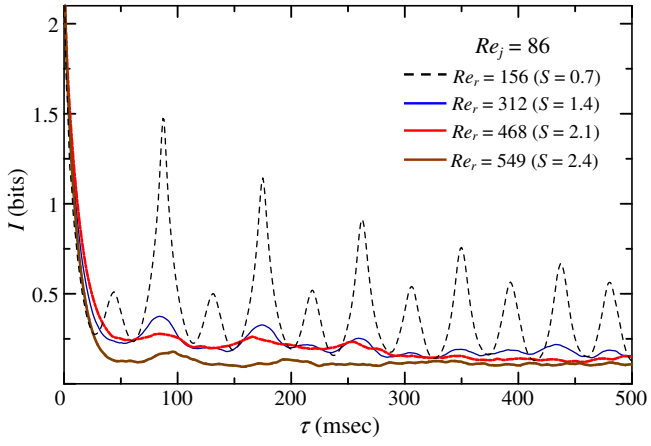

Fig. 5. Variations in mutual information as a function of time lag τ for different Re_r at Re_j = 86.

peak appear alternately every 90 msec, corresponding to the peaks observed in the power spectra. When Re_r increases up to 312, I rapidly decays at 40 ms and markedly decreases with the time lag, while fluctuating with a small amplitude at nearly the same period ($\approx$ 90 ms) as that at $Re_r = 156$. The dynamic instability as a result of information loss can be seen in the flame motion regardless of the appearance of the periodic oscillation in the power spectrum. With a further increase in N to $Re_r = 549$ ($S = 2.4$), a spontaneous and exponential loss of information that is likely to be caused by the onset of deterministically chaotic oscillation is clearly observed, indicating a significant increase in dynamic instability. The dimension related to the irreducible degrees of freedom in the attractor is one of the most significant dynamic properties for understanding the amount of complexity in the dynamic instability of the flame motion. The nonlinear characteristics of the dynamic instability that appears in the decay of the mutual information are thus discussed by estimating the correlation dimension in the attractor as follows.

The relationship between $\log C(\varepsilon)$ and $\log \varepsilon$ as a function of the embedding dimension up to $D = 10$ at $Re_r = 81$ ($S = 0.35$) is shown in Fig. 6(a). For each embedding dimension, the correlation of $\log C(\varepsilon)$ with $\log \varepsilon$ is indicated by a straight line, and the correlation dimension can be estimated from the gradient of the line. Here, note that similarly to in previous studies [18,29], the region in which the gradient of $\log C(\varepsilon)$ in the plot against $\log \varepsilon$ is constant is used to determine the correlation dimension in this work. The variation in the correlation dimension D_c with embedding dimension D is shown in Fig. 6(b). D_c approaches approximately unity with increasing D, and the dynamic behavior of the flame front at $Re_r = 81$ can be evaluated qualitatively to be periodic oscillation. If the time variation in Δr_f is completely random, D_c increases linearly with D as shown by the dotted straight line. This means that no deterministic nature in the constructed phase space can be observable. However, in this work, the values of D_c for all Re_r do not follow the straight line and saturate at a certain value with increasing D. The three-dimensional attractor ($\Delta r_f(t_i)$, $\Delta r_f(t_i + \tau_0)$, $\Delta r_f(t_i + 2\tau_0)$) and the saturated D_c at $Re_j = 86$ are shown as functions of Re_r or S in Fig. 7. Under the swirling condition of $Re_r \leqslant 156$, the shape of the attractor remains in a limit cycle with a small width and D_c is approximately unity, indicating periodic oscillation. At $Re_r = 237$ ($S = 1.1$), the trajectory of the attractor seems to shift to a torus and D_c approaches approximately 2, indicating quasi-periodic oscillation. When the spiral flame clearly starts to appear at $Re_r = 312$, the shape of the attractor becomes more complicated and D_c has a noninteger value, indicating deterministic chaos. The important point to note is that the values of D_c at $Re_r \geqslant 312$ are about 2.4. A nonlinear ordinary equation with three degrees of freedom, that is, the Lorenz equation theoretically derived from vorticity and energy equations under a free boundary condition, is often used in thermal and fluid physics as an important indicator for understanding the nonlinear characteristics of the dynamic instability in unstable phenomena generated by buoyancy-driven hydrodynamic instability. Although the Lorenz equation is not appropriate for representing the flame dynamics, it can be useful as an indicator for discussing the amount of complexity of the dynamic instability. The deterministic chaos produced by the Lorenz equation is treated as low-dimensional chaos, and its correlation dimension is about 2.1 [26,27]. On this basis, the dynamic instability of the chaotic oscillation in the flame front observed in this work can be concluded to be low-dimensional deterministic chaos. These results clearly show that with increasing Re_r, the flame motion undergoes a transition from periodic oscillation to low-dimensional chaos through quasi-periodic oscillation, and the occurrence of the spiral flame becomes significant to induce chaotic oscillation of the flame front. These results also show that the analytical method used in this work is valid for quantifying complex flame motion. In this work, the dynamic behavior of the flame front can be satisfactorily quantified with respect to its geometric characteristics. In addition to the correlation dimension, the Lyapunov exponent [15–20] or parallel trajectory method [22], which is used to estimate the orbital instability in the attractor, is also expected to be a powerful nonlinear analysis tool for obtaining more information on the dynamic instability.

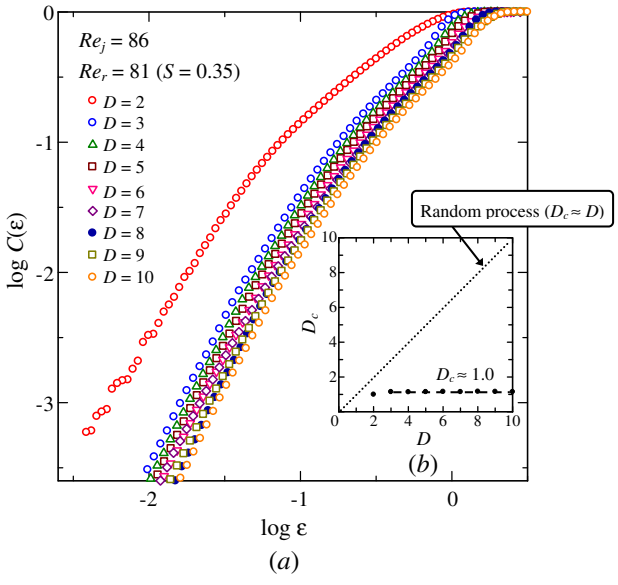

Fig. 6. (a) Correlation integral $\log C(\varepsilon)$ versus radius of hypersphere $\log \varepsilon$ for embedding dimension D at $Re_r = 81$ and $Re_j = 86$. (b) Correlation dimension D_c versus embedding dimension D.

As mentioned in Section 1, the vortex motion generated by the centrifugal instability associated with a rotating Taylor–Couette flow may cause irregular fluctuations in the flame front dynamics [14]. Revealing the relevance of the above vortex motion to the onset of the spiral flame leading to deterministic chaos is of importance for gaining a better understanding of the dynamic behavior of the flame front. In this work, we discuss the effect of the flow field on the onset of the spiral flame, focusing on how the flow field in the cold surrounding air around the burner tube exit changes with increasing rotational Reynolds number. The temporal evolution of the TiO_2 particles visualized by a laser tomographic method is shown in Fig. 8. At $Re_r = 156$, the trajectory of the TiO_2 particles does not change significantly with time and is similar to that obtained for the non-swirling flame ($Re_r = 0$). This means that under the swirling condition up to $Re_r = 156$, the rotation of the burner tube is not sufficient to affect the buoyancy-induced hydrodynamic instability. As a result, the periodic oscillation in the flame front remains unchanged under a low swirling flow. In contrast, when the spiral flame starts to appear at $Re_r = 312$, an interesting vortical structure appears on the surface of the burner tube. The vortex moves downstream by the entrainment effect due to the upward buoyant flow, and interacts with the flame front at the flame base. This flame/vortex interaction observed in this work has not yet been investigated experimentally in fundamental combustion research. On the basis of the results of our recent numerical simulation [14], it is verified that the vortical structure in the surrounding air can be attributed to the centrifugal instability associated with a rotating Taylor–Couette flow. With a further increase in Re_r to 468, the vortex merges with a newly generated vortex, and the scale of the vortex becomes significantly large to have a stronger effect on both the flame front and the interface between the hot combustion products and the cold surrounding air. The motion of the vortical structure appears to be temporally and spatially

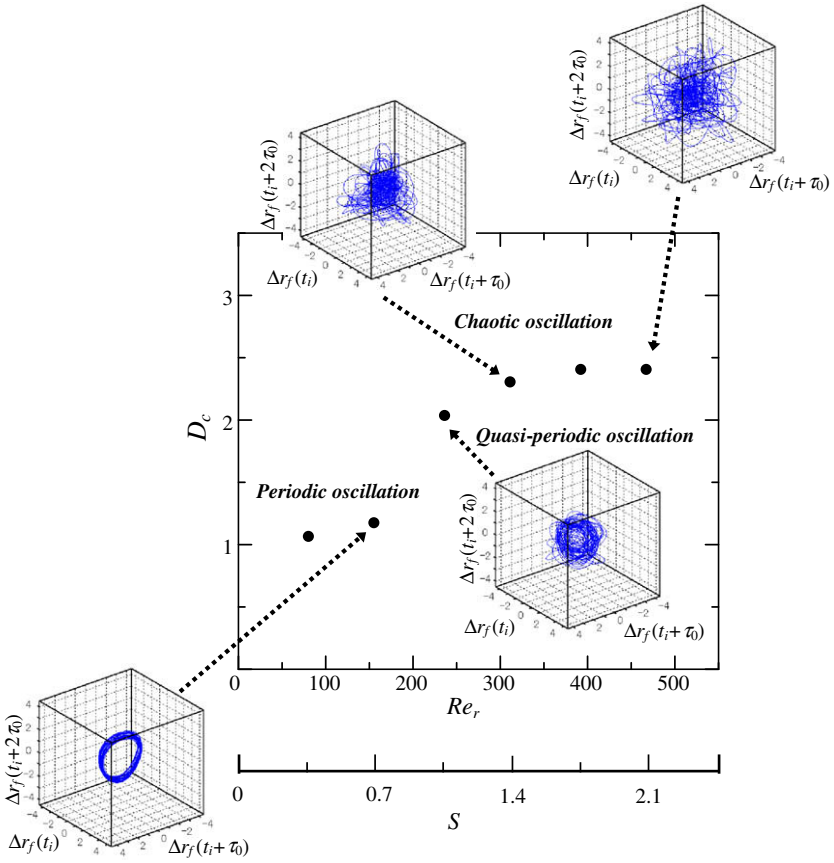

Fig. 7. Three-dimensional attractor ($\Delta r_f(t_i)$, $\Delta r_f(t_i+\tau_0)$, $\Delta r_f(t_i+2\tau_0)$) and the saturated value of D_c as a function of Re_r or S at $Re_j = 86$.

chaotic, and the vortex interacts irregularly with both the flame front and the interface. With respect to an experimental investigation on the dynamic behavior of a rotational Taylor–Couette flow consisting of a viscous fluid between two concentric cylinders, von Stamm et al. [30] reported that low-dimensional deterministic chaos appears throughout the torus scenario in the flow field and that its correlation dimension varied from about 2.1 to 2.5. As shown in Fig. 7, the values of the correlation dimension correspond to those obtained in ref. [30]. Although the ratio of gap length to gap width in a Taylor–Couette flow system does not correspond to that of this work, it is conceivable that the motion of Taylor-like vortices that form around the flame base has a strong effect on producing the low-dimensional chaotic oscillation of the flame front.

To conduct a more comprehensive investigation of the effect of Taylor-like vortices on the dynamic behavior of the flame front, we investigate the change in the correlation dimension D_c with increasing Swirl number S under the condition that the surface of the burner tube is not rotated. (Note that the solid-body rotation is induced in the fuel flow without rotating the surface of the burner tube.) As shown in Fig. 9, it is clear that both the shape of the trajectories in the attractor and D_c at $Re_r = 0$ remain nearly unchanged regardless of S, indicating periodic oscillation. This clearly shows that without the Taylor-like vortices/flame front and the interface interaction around the flame base, the motion of the flame cannot switch from periodic to chaotic oscillation even under a high swirling flow condition. Therefore, it is concluded that the motion of the Taylor-like vortices in the surrounding air plays an important role in the onset of a spiral flame leading to deterministically chaotic oscillation. Interestingly, the result in Fig. 9 also shows that the swirl of the fuel is insensitive to the flame dynamics generated by the buoyancy-driven hydrodynamic instability. This supports findings that the swirl of the surrounding air significantly affects the flame dynamics of a buoyancy-driven flickering flame [9,31].

As depicted in Fig. 4, the power spectrum of the low-dimensional chaotic oscillation of the flame front at $Re_r = 312$ exhibits low frequencies of less than 10 Hz, in addition to a large peak caused by the buoyancy-driven hydrodynamic shear layer instability. On the basis of the result shown in Fig. 9, the fluctuation generated by the collision of the Taylor-like vortices with the flame base is thought to be related to the onset of these low frequencies. We thus measure the collision frequency of the Taylor-like vortices from the time series images obtained by the laser tomographic method and elucidate the effect of Taylor-like vortices on the occurrence of low-dimensional deterministic chaos. The frequency of the collisions is estimated as $f_c(=1/(t_{j+1} - t_j))$, where t_j is the time at which a Taylor-like vortex collides with the flame base, t_{j+1} is the time at which a Taylor-like vortex next collides with the flame base, $j = 1, 2, 3, \ldots, n_c$, and n_c is the number of collisions). The probability distributions of the collision frequency f_c at $Re_r = 312$ and 549 are shown in Fig. 10. Under each condition, the probability is calculated from 100 items of data. At $Re_r = 312$, the probability distribution is within the frequency region lower than 7.5 Hz, and the probability is high around 5 Hz. These frequencies partially correspond to those of Δr_f as shown in Fig. 4. At $Re_r = 549$, the frequency region is broader and reaches 9.4 Hz. In addition to the relatively high probability approximately around 6 Hz, two peaks of the probability distribution are observed at 3.0 and 8.2 Hz, which are nearly in accord with those of Δr_f. This clearly shows that the collision of Taylor-like vortices with the flame base creates some of the low frequencies included in the chaotic oscillation of the flame front. The physical interpretation based on the flow visualization

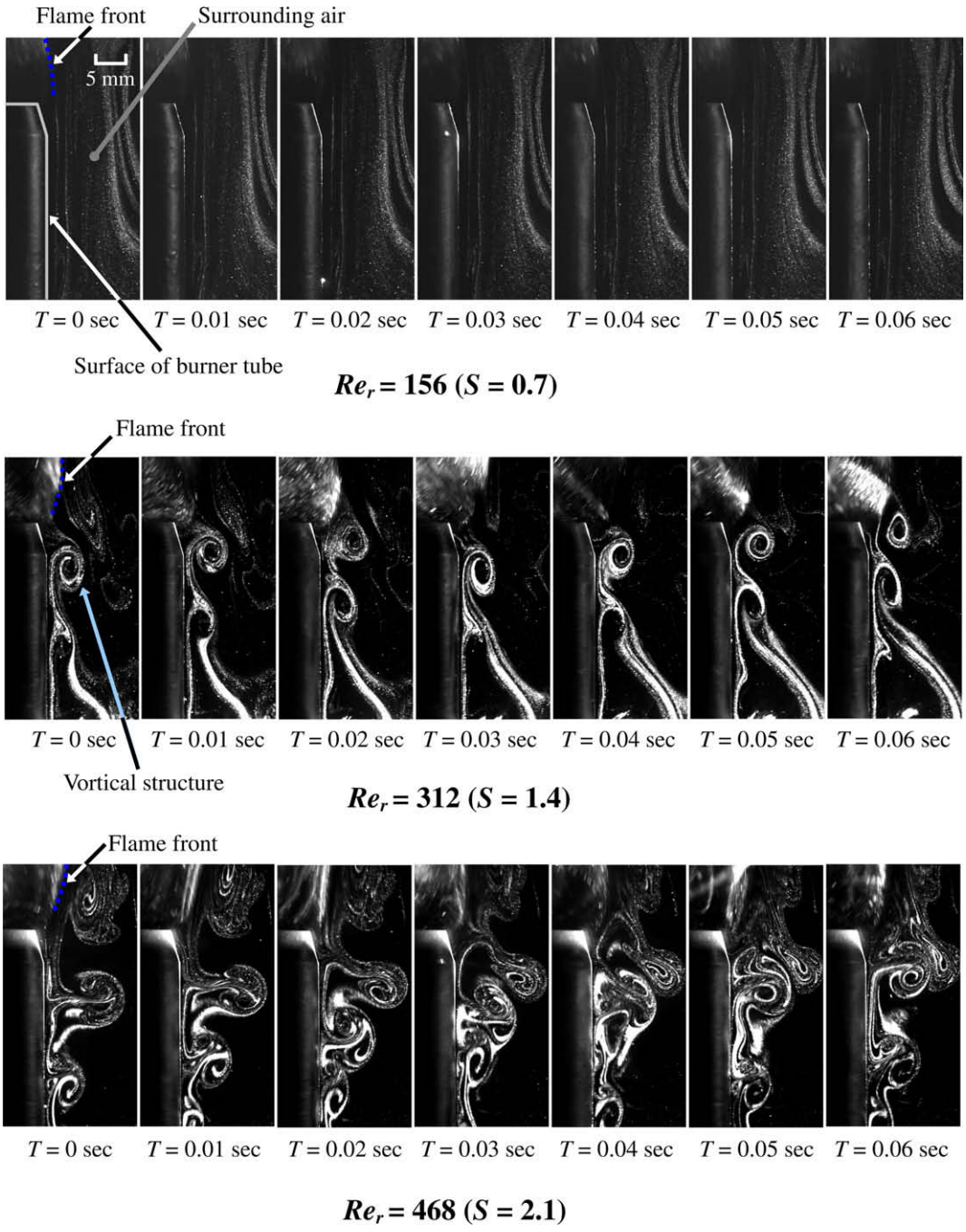

Fig. 8. Temporal evolution of the path of visualized particles in the surrounding air around the burner tube for different Re_r at $Re_j = 86$.

demonstrates that the fluctuation with low frequencies due to the collision of Taylor-like vortices with the flame base is superimposed on the periodic oscillation generated by the buoyancy-induced hydrodynamic instability, resulting in low-dimensional chaos in the flame dynamics. These results provide significant insights for understanding the buoyancy-driven flame instability under a swirling flow. In this work, we presented the dynamic behavior of the flame front under a swirling flow, focusing on the characterization of the flame dynamics from the viewpoint of nonlinear time series analysis. To elucidate the detailed mechanism of the chaotic oscillation of the flame front, the effect of Taylor-like vortices on the interface between the hot combustion products and the surrounding air will be examined in our next work.

5. Conclusions

The dynamic behavior of the buoyancy-induced flame oscillation under a swirling flow has been experimentally investigated from the viewpoint of nonlinear dynamics, focusing on how the dynamic behavior of the flame front changes with increasing rotational Reynolds number Re_r. Methane was used as the fuel in this work. The Reynolds number of the fuel jet Re_j was between 58 and 144, and the rotational Reynolds number Re_r was varied up to 550.

The buoyancy-induced flame oscillation remains nearly unchanged under a swirling flow condition up to $Re_r = 156$ (Swirl number $S = 0.7$). In contrast, when Re_r exceeds 312 ($S = 1.4$), irreg-

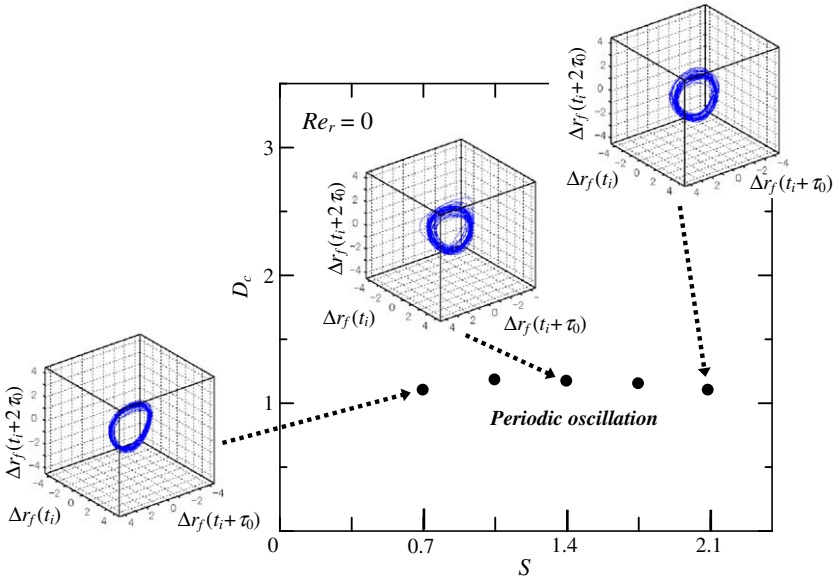

Fig. 9. Three-dimensional attractor ($\Delta r_f(t_i)$, $\Delta r_f(t_i+\tau_0)$, $\Delta r_f(t_i+2\tau_0)$) and the saturated value of D_c as a function of S at $Re_j = 86$ and $Re_r = 0$ under the condition that the surface of the burner tube does not rotate.

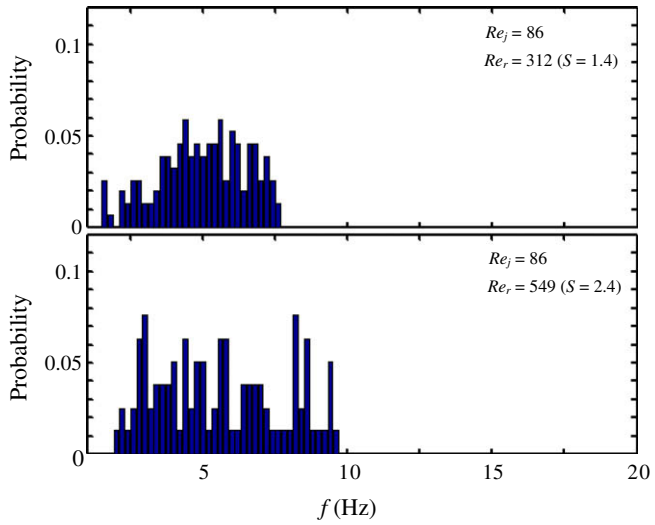

Fig. 10. Probability distributions of the collision frequency of Taylor-like vortices at $Re_r = 312$ and 549.

ular fluctuations of the flame front begin to be produced with the onset of a spiral flame. The formation of the spiral flame becomes increasingly prominent with the further increase in Re_r to 549 ($S = 2.4$), resulting in the nonperiodic oscillation of the flame front. The nonlinear character of the dynamic instability of the flame front is evaluated by sophisticated nonlinear time series analysis involving the attractor and the correlation dimension D_c which has not been widely applied to the investigation of combustion phenomena. For $Re_r \leqslant 156$, the attractor remains in a limit cycle and D_c is estimated to be about unity, indicating periodic oscillation. Upon increasing Re_r to 237 ($S = 1.1$), the trajectories of the attractor appeared to be rolled up and D_c approaches approximately 2, indicating quasi-periodic oscillation. When the spiral flame clearly appears at $Re_r = 312$, the trajectory of the attractor changes to a complicated structure and D_c becomes a noninteger value, indicating low-dimensional deterministic chaos. These results clearly demonstrate that the dynamic behavior of the buoyancy-induced flame oscillation changes from periodic to low-dimensional deterministic chaos through quasi-periodic oscillation with increasing rotational Reynolds number. Nonlinear time series analysis based on chaos theory was also shown to be valid for quantifying the characteristics of the complex flame instability. The flow visualization obtained by a laser topographic method shows that the vortex motion generated by the centrifugal instability associated with a rotating Taylor–Couette flow has a significant effect on inducing the low-dimensional deterministic chaos of the flame front.

Acknowledgments

One of the authors (H.G.) is partially supported by a "Research Grant from the Mazda Foundation", "Research Grant from Kurata Hitachi Science Technology Foundation", "CASIO Science Foundation", "Sasakawa Scientific Research Grant from The Japan Science Society" and a "Grant-in-Aid for Young Scientists (B) from the Ministry of Education, Culture, Sports, Science and Technology of Japan (MEXT)". The authors are very grateful to S. Mazubara (Ritsumeikan University) for his assistance in conducting the experiments. The authors thank Professor Kozo Saito (University of Kentucky) for his comments regarding our paper.

References

[1] L.D. Chen, J.P. Seaba, W.M. Roquemore, L.P. Goss, Buoyant diffusion flame, Proc. Combust. Inst. 22 (1988) 677–684.
[2] V.R. Katta, W.M. Roquemore, Role of inner and outer structures in transitional jet diffusion flame, Combust. Flame 92 (1993) 274–282.
[3] A.F. Ghoniem, I. Lakkis, M. Soteriou, Numerical simulation of the dynamics of large fire plumes and the phenomenon of puffing, Proc. Combust. Inst. 27 (1996) 1531–1539.
[4] D. Durox, T. Yuan, F. Baillot, J.M. Most, Premixed and diffusion flames in a centrifuge, Combust. Flame 102 (1995) 501–511.
[5] H. Sato, G. Kushida, K. Amagai, M. Arai, Numerical analysis of the gravitational effect on the buoyancy-driven fluctuations in diffusion flames, Proc. Combust. Inst. 29 (2002) 1671–1678.
[6] D. Durox, T. Yuan, E. Villermaux, The effect of buoyancy on flickering in diffusion flames, Combust. Sci. Technol. 124 (1997) 277–294.
[7] B.M. Cetegen, Y. Dong, Experiments on the instability modes of buoyant diffusion flames and effects of ambient atmosphere on the instabilities, Exp. Fluids 28 (2000) 546–558.
[8] H. Gotoda, S. Kawaguchi, Y. Saso, Experiments on dynamical motion of buoyancy-induced flame instability under different oxygen concentration, Exp. Therm. Fluid Sci. 32 (2008) 1759–1765.

[9] R.F. Huang, S.C. Yen, Aerodynamic characteristics and thermal structure of nonpremixed reacting swirling wakes at low Reynolds numbers, Combust. Flame 155 (2008) 539–556.
[10] J.M. Cha, S.H. Sohrab, Stabilization of premixed flames on rotating Bunsen burners, Combust. Flame 106 (1996) 467–477.
[11] S. Ishizuka, Flame propagation along a vortex axis, Prog. Energy Combust. Sci. 28 (2002) 477–542.
[12] H. Gotoda, T. Ueda, I.G. Shepherd, R.K. Cheng, Flame flickering frequency on a rotating Bunsen burner, Chem. Eng. Sci. 62 (2007) 1753–1759.
[13] H. Gotoda, K.H. Chuah, G. Kushida, Effect of swirl on flickering motion of diffusion flame, in: 59th Annual Meeting of the Division of Fluid Dynamics, American Physical Society, FL, USA, 2006, pp. 186–186.
[14] K.H. Chuah, H. Gotoda, G. Kushida, Numerical simulations of methane diffusion flame with burner rotation, Progress in Scale Modeling, Springer-Verlag, New York, 2008. pp. 211–218.
[15] H. Koizumi, Laminar-turbulent transition behavior of fully developed air flow in a heated horizontal tube, Int. J. Heat Mass Transfer 45 (2002) 937–949.
[16] S.F. Wang, R. Mosdorf, M. Shoji, Nonlinear analysis on fluctuation feature of two-phase flow through a T-junction, Int. J. Heat Mass Transfer 46 (2003) 1519–1528.
[17] R. Mosdorf, P. Cheng, H.Y. Wu, M. Shoji, Non-linear analysis of flow boiling in microchannels, Int. J. Heat Mass Transfer 48 (2005) 4667–4683.
[18] M. Shoji, Y. Takagi, Bubbling features from a single artificial cavity, Int. J. Heat Mass Transfer 44 (2001) 2763–2776.
[19] T.J. Lin, R.C. Juang, Y.C. Chen, C.C. Chen, Predictions of flow transitions in a bubble column by chaotic time series analysis of pressure fluctuation signals, Chem. Eng. Sci. 56 (2001) 1057–1065.
[20] J.T. Cieslinski, R. Mosdorf, Gas bubble dynamics – experiment and fractal analysis, Int. J. Heat Mass Transfer 48 (2005) 1808–1818.
[21] H. Gotoda, T. Ueda, Transition from periodic to non-periodic motion of a Bunsen-type premixed flame tip with burner rotation, Proc. Combust. Inst. 29 (2002) 1503–1509.
[22] H. Gotoda, T. Ueda, Orbital instability and prediction of a Bunsen flame tip motion with burner rotation, Combust. Flame 140 (2005) 287–298.
[23] H. Gotoda, Y. Saso, Unsteady motion of pool fire on small-scale burner, Int. J. Bifurcat. Chaos 17 (2007) 2185–2193.
[24] A.M. Fraser, H.L. Swinney, Independent coordinates for strange attractors from mutual information, Phys. Rev. A 33 (1986) 1134–1140.
[25] F. Takens, Dynamical systems of turbulence, in: Lecture Notes in Mathematics, vol. 898, Springer-Verlag, New York, 1981, pp. 366–381.
[26] P. Grassberger, I. Procaccia, Measuring the strangeness of strange attractors, Physica D 9 (1983) 189–208.
[27] P. Grassberger, I. Procaccia, Characterization of strange attractors, Phys. Rev. Lett. 50 (1983) 346–349.
[28] S. Kadowaki, N. Ohkura, Time series analysis on the emission of light from methane-air lean premixed flames: diagnostics of the flame instability, Trans. Jpn. Soc. Aeronaut. Space Sci. 51 (2008) 133–138.
[29] J.P. Barnard, C. Aldrich, M. Gerber, Identification of dynamic progress systems with surrogate data methods, AIChE J. 47 (2001) 2064–2075.
[30] J. von Stamm, U. Gerdts, T. Buzug, G. Pfister, Symmetry breaking and period doubling on a torus in the VLF regime in Taylor–Couette flow, Phys. Rev. E 54 (1996) 4938–4957.
[31] K.H. Chuah, G. Kushida, The prediction of flame heights and flame shapes of small fire whirls, Proc. Combust. Inst. 31 (2007) 2599–2606.